Journal of Stress Analysis
Vol. 9, No. 2, 2025, 31-39

ORIGINAL RESEARCH PAPER

Numerical Investigation and Comparison of Temperature and Residual Stress in FSW and UFSW Processes of Two Heterogeneous Aluminum Alloys

Maziar Mahdipour[a,*], **Amir Ghiasvand**[b]

[a] Department of Mechanical Engineering, Kermanshah University of Technology, Kermanshah, Iran.
[b] Department of Mechanical Engineering, Tabriz University, Tabriz, Iran.

Article info

Article history:
Received 2025-04-21
Received in revised form 2025-06-15
Accepted 2025-06-23

Keywords:
Friction Stir Welding (FSW)
Underwater Friction Stir Welding (UFSW)
Residual stresses
Numerical simulation
Aluminum alloys

Abstract

Friction stir welding (FSW) is classified as a solid-state joining method with no melting of the workpiece and tool. The affecting factors for creating a joint in this method are the generated heat, pressure, and large deformations in the workpiece. The generation and appropriate distribution of heat in the FSW process guarantee the creation of a high-quality and defect-free joint. One of the modifications that are used to adjust the temperature distribution to other zones of the workpiece is the usage of the Underwater Friction Stir Welding (UFSW) technique. In the present study, the FSW and UFSW processes have been numerically investigated using the indirect process simulation technique and the applied heat flux coding through the DFLUX subroutine, and the results of the temperature distribution and residual stress in the joined samples obtained using these two techniques have been compared. According to the results, it was found that the temperature distribution patterns in the FSW and UFSW processes differ significantly from each other, and these changes in the temperature distribution of the workpiece ultimately lead to a significant difference in the temperature pattern in the weld cross-section and the longitudinal and transverse residual stresses in the specimens joined by the two techniques.

Nomenclature

Q_{pin}	Heat generated by the tool pin	$Q_{shoulder}$	Heat generated by the tool shoulder
H_{pin}	Tool pin height	R_{Tpin}	Tool pin radius at shoulder
R_{Bpin}	Tool pin radius at pin bottom	$R_{shoulder}$	Tool shoulder radius
F_z	Vertical force applied to the tool	A_{Bpin}	Area of the bottom of the pin
ω	Tool rotational speed	σ_{yield}	Yield stress of the workpiece
α	Tool shoulder indented angle	μ	Coefficient of friction
AS	Advancing Side	RS	Retreating Side
HAZ	Heat Affected Zone		

*Corresponding author: M. Mahdipour (Assistant Professor)
E-mail address: M.mahdipour@kut.ac.ir
doi: 10.22084/JRSTAN.2026.32471.1281
ISSN: 2588-2597

1. Introduction

FSW is classified as a solid-state joining process, in which no melting occurs in the workpiece and the tool [1]. The two main factors affecting solid-state joining are pressure and large plastic deformations. Many categories of solid-state joining exist which work based on the factors causing pressure and deformation [2]. The FSW process was invented in 1991 at the TWI Institute [3] and today this method is used in many industries. The motivation for the invention of FSW was the existence of numerous limitations and defects in the joining and welding of aluminum alloys with common techniques. By using FSW in aluminum alloys, defects are eliminated and the joint efficiency is increased [2]. Dissimilar aluminum alloy joints have attracted increasing attention in recent years due to their high strength-to-weight ratio and corrosion resistance in engineering applications [4, 5]. Heat and plastic deformation are the two main factors shaping the plastic flow in the workpiece which can have dual effects on the quality of the joint. If these two factors are properly controlled, the quality of the joint will increase, otherwise, changing each of the mentioned factors from the allowable range will lead to different defects in the weld [6]. Therefore, accurate prediction of temperature history and residual stress distribution is essential for evaluating the mechanical performance of FSW joints. In this regard, numerical simulation has become a valuable tool for understanding the complex thermo-mechanical behavior of the process. One of the issues that must be considered in the FSW process is the increase in temperature in areas away from the weld zone, which can lead to large tensile residual stresses in the workpiece and make some areas susceptible to defects [7]. Among the modifications taken to adjust the temperature distribution to other areas of the workpiece is the use of the UFSW technique [8]. Using the UFSW technique, the thermal conditions of areas away from the weld section can be adjusted and possible defects in these areas can be prevented [9].

Recent studies have shown that UFSW significantly reduces peak temperature, narrows the HAZ, limits excessive grain growth, improves mechanical properties due to enhanced convective heat transfer, and reduces welding-induced residual stresses and distortion [10, 11]. However, the relationship between cooling conditions and residual stress evolution is still not fully clear, especially for dissimilar aluminum alloys [11, 12].

Due to the existence of numerous variables involved in the process affecting the quality of the joint in FSW and UFSW processes, many experimental, analytical, and numerical investigations have been carried out; however, there is still a need for further studies in this field. Zhang et al. presented a three-dimensional thermal model for the UFSW process and confirmed the accuracy of the model by comparing the model results with the experimental results [13]. Based on the results, the maximum temperature in UFSW was greatly reduced compared to that in FSW. Chandan et al. conducted an experimental study of the UFSW process under different rotational speeds and reservoir water heights and compared the residual stresses in the samples created in the two conditions of FSW and UFSW and found that the defects formed in the UFSW process are much less than those in the FSW process [14]. Zhang et al. studied the FSW and UFSW of aluminum–copper joints experimentally and found that the maximum temperature value and the time of thermal cycles created in the UFSW process are significantly lower than those in FSW [15]. In another study, Sabari et al. investigated the FSW and UFSW processes experimentally and numerically and estimated the temperature distribution in the TMAZ (Thermo-Mechanically Affected Zone) for both processes using two different approaches [16]. Similarly, Maharia et al. studied the temperature distribution created in the process using finite element simulation of the FSW and UFSW processes [17].

Based on the obtained results, the temperature distributions beneath the tool shoulder are approximately the same in both processes, but in other areas of the workpiece, the maximum temperature generated by the UFSW process is lower than that of FSW. Although these studies have contributed to understanding the thermal behavior of FSW and UFSW processes, most of them focus on either experimental observations or temperature prediction, while comprehensive numerical comparisons of residual stress evolution in dissimilar AA6061-T6/AA5086-O joints remain limited.

In recent years, numerical simulation has become a valuable tool for understanding the complex thermo-mechanical behavior of FSW. Compared with expensive and time-consuming experimental studies, finite element (FE) modeling can predict the temperature history, distribution, plastic deformation, material flow, and the residual stress distribution under different welding conditions. Recent advances in coupled thermo-mechanical models, including Coupled Eulerian-Lagrangian (CEL) and sequentially coupled finite element approaches, have significantly improved the prediction accuracy of thermal fields and residual stress distributions [12, 18]. Consequently, numerical simulation has become an effective tool for optimizing process variables and improving the structural integrity of FSW components [19].

Despite significant advances in numerical modeling of FSW and UFSW processes, limited studies have simultaneously investigated both thermal fields and residual stress distribution in dissimilar aluminum alloy joints.

Unlike previous studies that primarily focus on either thermal analysis or partial validation of temperature fields, the present study provides a fully coupled thermo-mechanical analysis and a systematic numerical comparison of both thermal evolution and residual stress distribution in dissimilar AA6061-T6/AA5086-O joints under identical welding conditions for the FSW and UFSW processes.

Therefore, the main objective of this study is to numerically investigate and compare the thermo-mechanical behavior of dissimilar AA6061-T6/AA5086-O aluminum alloy joints produced by FSW and UFSW. The study focuses on the evolution of temperature fields, residual stress distributions, and weld zone characteristics under identical conditions to provide a consistent and direct comparison between the two welding techniques. In this manner, a three-dimensional coupled thermo-mechanical FE model was developed using ABAQUS software. The moving heat source is implemented through a DFLUX subroutine to accurately simulate the transient heat generation accurately during the welding process. The model can predict the thermal histories and temperature distributions, as well as residual stress distributions, allowing a detailed assessment of the influence of underwater cooling on stress distribution in dissimilar aluminum alloy joints.

The main contributions of this study can be summarized as follows:

- Development of a unified FE model to simulate both FSW and UFSW under identical welding conditions
- Comparative analysis of thermal and residual stress distributions in dissimilar AA6061-T6/AA5086-O joints
- Evaluation of the effect of underwater cooling on the reduction and distribution of residual stresses
- Providing a mechanistic understanding of weld zone formation and thermo-mechanical behavior in dissimilar aluminum alloys.

2. Numerical Simulation

In order to investigate the numerical simulation of the FSW and UFSW processes, the ABAQUS finite element software was used. The numerical simulation was carried out based on the conditions and information including the tool geometry, process parameters, and workpiece and tool material, presented in an experimental work carried out by Jamshidi Aval et al. [20]. It should be noted that their research was only based on the FSW process, and in the present study, in addition to the FSW process, the UFSW process has been also be simulated.

The workpiece material in the FSW process consisted of two aluminum alloys AA6061-T6 and AA5086-O, according to the experimental work [20]. For this purpose, two separate parts were used to create a workpiece with dimensions of 5×50×150 mm. According to the experimental work, the tool used has a concave conical shoulder with an angle of 2 degrees and a radius of 20 mm along with a conical pin with an upper radius (radius at the interface with the shoulder) of 6 mm and a lower radius (radius of the bottom of the pin) of 3 mm. The tool rotation speed was considered to be 840 rpm, and its linear movement speed was also considered to be 150 mm/min. Due to the use of an indirect analysis, only the workpiece was modeled and by applying a moving heat flux to the workpiece, conditions similar to those in the FSW and UFSW processes were created. The pin dimensions were used as input data for the FORTRAN code in the DFLUX subroutine to specify the volume swept by the pin for the application of volumetric heat flux. Two different equations were used to apply the heat flux due to the pin and the tool shoulder, which were selected based on Schmidt's model [21]:

$$Q_{pin} = 2\pi\omega H_{pin}\frac{\sigma_{yield}}{\sqrt{3}}(\frac{R_{Tpin}+R_{Bpin}}{2}) + \frac{2}{3}\pi\omega\mu\frac{F_z}{A_{Bpin}}R^2_{Bpin} \quad (1)$$

$$Q_{shoulder} = \frac{2}{3}\pi\omega\frac{\sigma_{yield}}{\sqrt{3}}\ (R^3_{shoulder} - R^3_{Tpin})(1+\tan\alpha) \quad (2)$$

According to these equations and coding in the form of a DFLUX subroutine, two different heat fluxes were applied to the surface and the entire volume of the workpiece, a surface heat flux according to the heat generated by the shoulder using Eq. 1 on the upper surface of the workpiece and a volumetric heat flux based on Eq. 2 for the heat source generated by the tool pin was applied to the total volume of the workpiece so that the input heat of the process could be modeled through these two heat fluxes. To apply these two heat fluxes, coding was done in such a way that the magnitude of the applied heat fluxes could be defined depending on the spatial location and the time. It should be noted that the simulation of the tool plunge and withdrawal stages was omitted and only the joint creation step was considered and finally the problem was solved by linking the written code and ABAQUS software. The temperature-dependent thermal and mechanical properties of the AA6061-T6 and AA5086-O alloys are listed in Table 1 and Table 2, respectively.

The main difference in the numerical simulation of the two processes of FSW and UFSW is in applying the thermal boundary conditions. Different convective heat transfer coefficients were defined for different parts of the workpiece shown in Table 3 under the two welding conditions of FSW and UFSW . It should be noted that the ambient temperature in the simulation of the two processes was considered to be 25°C.

Table 1
Mechanical and thermal properties of AA6061-T6 alloy.

T °(c)	E (Gpa)	Yield Stress (MPa)	C_p ($Wm^{-2}K^{-1}$)	(kgm^{-3})ρ	$\alpha(10^{-6}°c^{-1})$
25	66.94	276	896	2690	23.5
100	63.21	262	978	2690	24.6
150	56.32	214	1004	2670	25.7
200	56.80	103	1028	2660	26.6
250	51.15	34	1052	2660	27.6
300	47.17	19	1078	2660	28.5
450	43.51	12	1133	2630	29.6

Table 2
Mechanical and thermal properties of AA5086-O alloy.

T °(c)	E (Gpa)	Yield Stress (MPa)	C_p ($Wm^{-2}K^{-1}$)	(kgm^{-3})ρ	$\alpha(10^{-6}°c^{-1})$
25	70	117	900	2657	23.8
250	67.8	38	960	2612	25.5
300	60.7	33.4	980	2607	26.8
400	51	19.5	1020	2593	28.9
500	37.4	10.3	1130	2590	31.5

Table 3
Convective heat transfer coefficients used.

Parameter	Unit	FSW	UFSW
h-upside	$W.m^{-2}.°C$	15	2000
h-downside	$W.m^{-2}.°C$	200	1000

According to the experimental work, in both processes, the AA6061-T6 alloy was placed on the advancing side and AA5086-O alloy on the retreating side. Considering that the travel speed was considered to be 150 mm/min and the length of the workpiece was also 150 mm, a transient thermal analysis step of 60 seconds was used to simulate the welding process, and in both FSW and UFSW models, a thermal analysis step of 340 seconds was used to cool the workpiece. After completing the thermal step and obtaining the results of the temperature distribution in the workpiece, a static analysis step of 400 seconds was used to estimate and simulate the mechanical behavior of the workpiece, and through this mechanical step, the residual stresses of the workpiece were obtained.

In order to mesh the model for both processes, 10500 elements from the DC3D8 family and C3D8R family were used in the thermal and mechanical analyses, respectively. To enhance the accuracy of the results, after the mesh sensitivity analysis was performed, the model was meshed in such a way that the element density was increased in the weld line area. Fig. 1 shows the mesh applied to the model.

In order to ensure the reliability of the numerical results and determine the optimal element size, a mesh sensitivity analysis was performed prior to conducting the thermo-mechanical simulations. Seven different mesh sizes, namely 6, 5, 4, 3, 2, 1, and 0.5 mm, were considered in the welding region. Since the regions far from the weld line experience relatively low thermal gradients, a biased mesh with gradually coarsening elements was employed outside the welding zone to reduce computational time.

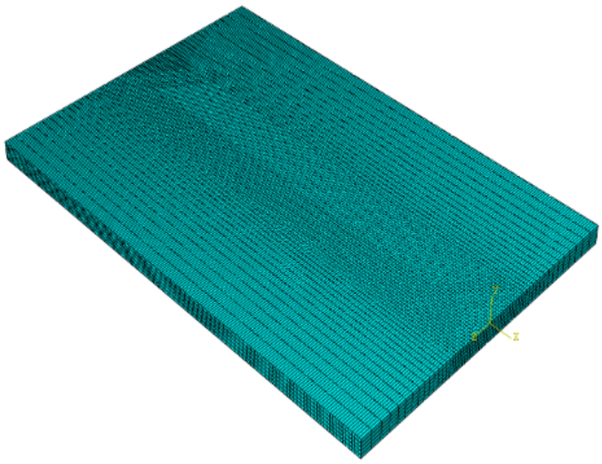

Fig. 1. Final model meshing.

Transient thermal analyses were carried out for both FSW and UFSW conditions. The peak temperature was selected as the mesh convergence criterion because temperature is a dominant parameter controlling material plasticization and subsequent thermomechanical behavior in friction stir welding processes.

Table 4 summarizes the effect of mesh size and the total number of elements on the predicted peak temperatures for both FSW and UFSW processes.

Furthermore, the variation of peak temperature with mesh size is illustrated in Fig. 2. As shown in Fig. 2, the predicted peak temperatures increase gradually with mesh refinement and become nearly constant for element sizes smaller than 1 mm.

For the FSW model, the predicted peak temperature changed only from 362 °C to 363 °C when the element size decreased from 1 mm to 0.5 mm. Similarly, in the UFSW model, the peak temperature increased from 281 °C to 283 °C. Despite these negligible changes in temperature, the total number of elements increased significantly from 46,500 to 138,000, resulting in a considerable increase in computational time.

Table 4
Results of mesh sensitivity analysis for FSW and UFSW simulations.

Mesh size (mm)	Total number of elements	Peak temperature (°C)	
		FSW	UFSW
6	2250	142	119
5	3000	195	143
4	4940	263	201
3	8500	313	252
2	19125	349	272
1	46500	362	281
0.5	138000	363	283

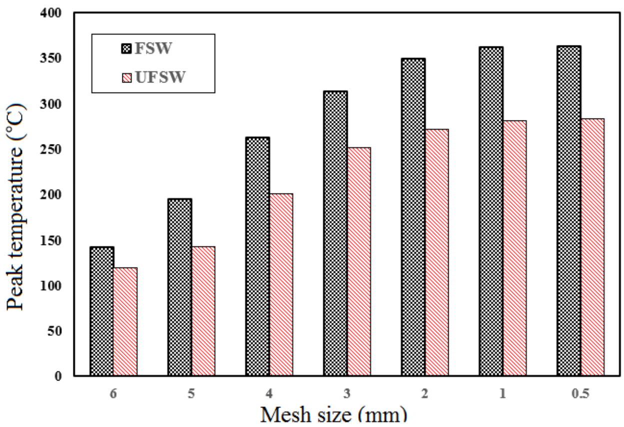

Fig. 2. Variation of peak temperature with mesh size for FSW and UFSW processes.

Therefore, considering both accuracy and computational efficiency, the element size of 1 mm in the welding region was selected as the optimal mesh size and used in all subsequent simulations.

3. Results and Discussion

3.1. Validation

In order to validate the results obtained from the numerical simulation, the numerical temperature measurements were compared with the experimental results of Jamshidi et al.'s work [20]. Table 5 shows the temperature measurements obtained at a point 10 mm away from the weld centerline on both the advancing and retreating sides.

According to the results presented in Table 5, it was determined that the numerical method used for the simulation of the FSW process is capable of correctly estimating the temperature values in the workpiece with high accuracy.

The obtained prediction errors (1.18% and 2.24%) are comparable to or lower than those reported in previous thermo-mechanical FSW simulations, indicating that the developed model provides satisfactory accuracy for predicting the thermal response of the welding process.

Table 5
Comparison of experimental and numerical results in the FSW process.

State	Temperature (°C)	
	Advancing side	Retreating side
Experimental [20]	338	312
Numerical	342	319
Error	1.18 %	2.24 %

3.2. Process Temperature

One of the main characteristics of welding processes is the maximum process temperature. The temperature in welding processes can have a detrimental or ebneficial effect. If the process temperature can be controlled within an appropriate range, the joint will have the best possible quality. In solid-state processes, the process temperature is generally 0.7 to 0.8 times the melting temperature of the parts [2]. If the temperature exceeds this range, the possibility of local melting during the process increases, and this phenomenon will lead to destructive defects in the joint. Fig. 3 shows the temperature history plot of the midpoint of the workpiece for the FSW and UFSW processes.

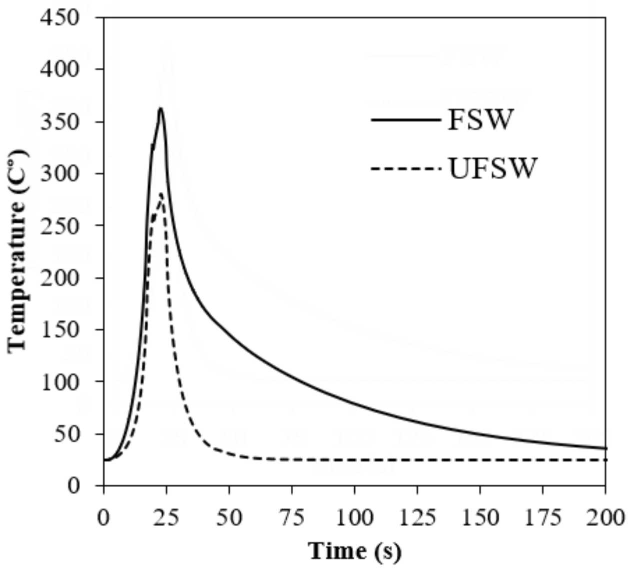

Fig. 3. Temperature history plot of FSW and UFSW.

According to Fig. 3, it can be seen that the temperature history curves in the two processes have two fundamental differences. First, the maximum temperature in the FSW process is significantly higher than that in the UFSW process due to the high heat concentration in the central weld zone and the lack of proper cooling during the welding operation. Second, due to the presence of fluid as a coolant in the UFSW process, the part returns to the ambient temperature in a much shorter time and this can lead to a decrease in the number of defects with thermal origin.

These findings are consistent with previous studies on UFSW, where the presence of a water medium increased the heat extraction rate and consequently reduced both the peak temperature and the cooling time. Zhang et al. [13] and Maharia et al. [17] similarly reported lower peak temperatures in UFSW compared with conventional FSW. The agreement between the present numerical predictions and previous investigations supports the capability of the developed model to capture the thermal response of both welding processes.

Fig. 4 shows the temperature distribution contour of the upper surface of the workpiece in the FSW and UFSW processes at the moment when the tool passes the midpoint of the workpiece.

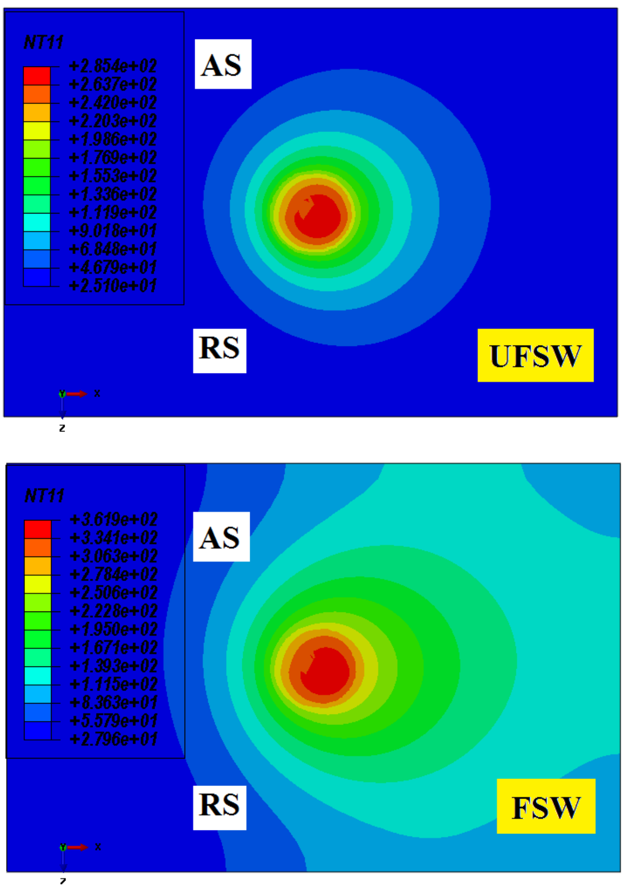

Fig. 4. Upper surface temperature distribution contour.

In the contours presented in Fig. 4, it can be seen that the higher temperatures in both FSW and UFSW processes are located on the harder alloy side (AA6061-T6) and the advancing side, namely the AA6061-T6 alloy, which is due to the higher thermal conductivity of this alloy compared to that of the AA5086-O alloy.

According to Fig. 4, after the tool passes along the weld line, the cooling process occurs at a very high rate in the UFSW process, which ultimately leads to a reduction in the thermal cycle time after the tool passes.

The observed reduction in thermal cycle duration is important because it directly affects microstructural evolution and residual stress development. Similar observations have been reported in recent studies, where enhanced cooling during UFSW resulted in a narrower HAZ and reduced thermal exposure of the surrounding material [10, 11].

Another fundamental difference between FSW and UFSW processes is the temperature distribution profile in the weld cross-section. Fig. 5 shows the temperature distribution contour in the weld cross-section for both processes.

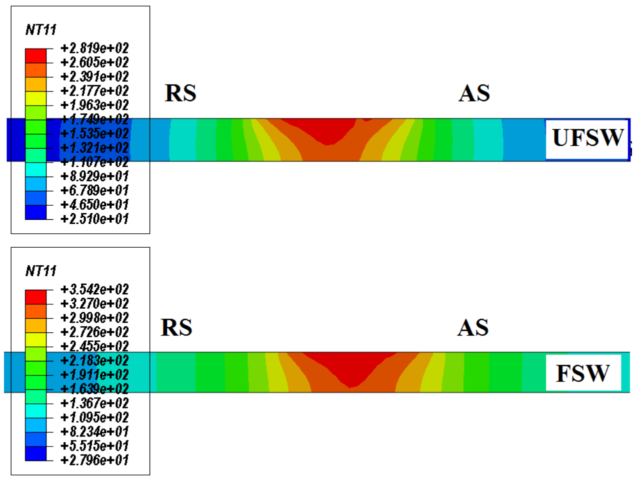

Fig. 5. Temperature distribution contour in the weld cross-section.

According to Fig. 5, the pattern of the temperature distribution in the area under the tool is the same in the two processes, but at locations further away from the tool in the weld cross-section, the temperature distribution in the two processes is completely different. In the FSW process, with increasing distance from the tool influence region, there is still a relatively high temperature distribution in the workpiece cross-section, which leads to an increase in the HAZ width. An increase in the width of the HAZ in welding processes is an undesirable event because the materials within in these regions, due to the relatively large thermal cycles, experience a decrease in their mechanical properties. This increase leads to a decrease in static and fatigue strength, as well as weld quality.

The narrower HAZ predicted for the UFSW process is in agreement with the findings reported in the literature, where higher cooling rates were shown to suppress grain growth and reduce thermal softening in aluminum alloys. Therefore, the thermal behavior predicted by the present model is consistent with the expected metallurgical response of UFSW joints.

3.3. Residual Stresses

Residual stresses are of particular importance in all welding processes. These residual stresses can be divided into two categories, namely tensile and compressive stresses. Generally, the presence of compressive residual stresses in the part enhances static and fatigue strength, but tensile residual stresses severely affect the fatigue life of welded samples and reduce the service life of the welded part. Therefore, controlling tensile stresses in the welded part, especially in the welding areas in different samples, is of great importance.

Although numerous studies have investigated temperature evolution during FSW and UFSW, comparatively fewer studies have provided a detailed analysis of residual stress development, particularly for dissimilar aluminum alloy joints. Therefore, numerical prediction of residual stresses remains an important research topic for evaluating the structural integrity and service performance of welded components.

In the present study, longitudinal and transverse residual stresses in the joints created by the FSW and UFSW processes were evaluated. Figs. 6 and 7 illustrate the longitudinal residual stresses (along the weld line) and transverse residual stresses (perpendicular to the weld line) of the joints produced by the FSW and UFSW processes at the end of the cooling, respectively.

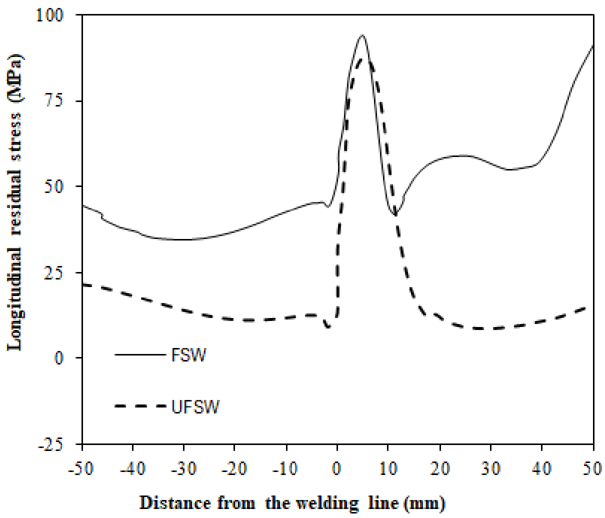

Fig. 6. Longitudinal residual stress plot in FSW and UFSW.

Based on Figs. 6 and 7, it was found that both longitudinal and transverse residual stresses in both processes at the end of the cooling step are tensile. According to the diagrams presented in both longitudinal and transverse positions, the residual stresses of the samples created by the UFSW technique are lower, which is due to the faster and more appropriate cooling of the part by the coolant.

Also as seen in Fig. 6, the longitudinal residual stress in the FSW is higher in the AA6061-T6 alloy section, which is due to the larger heat concentration at the location of this alloy, but it is observed that if a fluid-based cooling system is used, this difference in the residual stresses in the two samples is significantly reduced, and the longitudinal residual stress pattern in the two advancing and retreating sides become more similar at the end of the UFSW process.

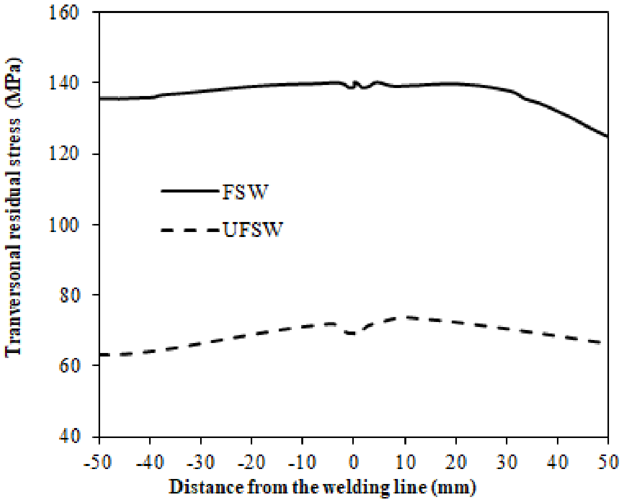

Fig. 7. Transverse residual stress plot in FSW and UFSW.

The more uniform residual stress distribution observed in UFSW can be attributed to the reduced thermal asymmetry across the weld region. Similar behavior has been reported in previous studies, where underwater cooling promoted a more homogeneous thermal field and consequently reduced stress concentration in localized regions.

Another noteworthy point about longitudinal residual stresses is the similarity of the residual stress values in the central zone of the weld for the FSW and UFSW processes. According to Fig. 6, the values of tensile residual stresses are almost the same for both processes in the tool shoulder region, which is due to the nearly identical temperature distribution, which was also observed in Fig. 5 as described in the previous section. It can be observed in Figs. 6 and 7 that a significant reduction in both longitudinal and transverse stress values has occurred in the samples joined by the UFSW method, and this reduction in residual stresses can be considered an important and effective factor in improving the quality of the joint.

The observed reduction in residual stresses under underwater conditions is consistent with previous experimental and numerical studies reported in the literature, which attribute this behavior to the enhanced cooling rate and the resulting reduction in thermal gradients during welding. The present results further demonstrate that underwater cooling not only decreases the magnitude of tensile residual stresses but also promotes a more uniform stress distribution across the welded joint, which is beneficial for improving structural reliability and fatigue performance.

Overall, the present results not only confirm the general thermal and mechanical trends reported in previous FSW and UFSW studies but also provide a systematic comparison of temperature evolution and residual stress distributions in dissimilar AA6061-T6/AA5086-O joints under identical welding conditions. Unlike many previous investigations that primarily focused on thermal behavior, the present study simultaneously evaluates thermal fields and residual stresses within a unified thermo-mechanical finite element framework, providing additional insight into the influence of underwater cooling on weld integrity.

4. Conclusion

In the present study, the temperature distribution and residual stresses in the FSW and UFSW processes were investigated using the ABAQUS finite element software. The heat flux was implemented using the DFLUX subroutine, and the following results were obtained:

- The maximum temperature level in the FSW process is significantly higher than in the UFSW process due to high heat concentration at the central weld zone and insufficient cooling during welding.
- The higher temperatures in both FSW and UFSW processes are located on the harder alloy side (advancing side, namely the AA6061-T6 alloy), which is due to the higher thermal conductivity of this alloy compared to that of the AA5086-O alloy during the process.
- The temperature distribution pattern in the area under the tool is the same in the two processes, but the temperature distribution at locations farther from the tool in the weld cross-section of the two processes is completely different. In the FSW process, there is still a relatively high temperature distribution in the cross-section of the workpiece with distance from the tool presence area, which significantly increases the width of the HAZ in the workpiece.
- In the UFSW process, both longitudinal and transverse residual stresses values are lower than those in FSW.
- Longitudinal residual stresses in the FSW process were higher in the AA6061-T6 alloy section, which is due to the larger heat concentration at the location of this alloy.
- Based on the results, a significant reduction in both longitudinal and transverse stress values has occurred in the samples joined by the UFSW process.

References

[1] Ghiasvand, A. and S. Hassanifard, Numerical simulation of FSW and FSSW with pinless tool of AA6061-T6 Al alloy by CEL approach. 2018.

[2] Mishra, R.S., P.S. De, and N. Kumar, Friction Stir Processing, in Friction Stir Welding and Processing: Science and Engineering, R.S. Mishra, P.S. De, and N. Kumar, Editors. 2014, Springer International Publishing: Cham. p. 259296.

[3] Thomas, W.M., Friction stir welding. International Patent Appl. N PCT/GB92/02203, 1991.

[4] Ghiasvand, A., M. Kazemi, M. Mahdipour Jalilian, and H. Ahmadi Rashid, Effects of tool offset, pin offset, and alloys position on maximum temperature in dissimilar FSW of AA6061 and AA5086. International Journal of Mechanical and Materials Engineering, 2020. 15(1): p. 6.

[5] Ghiasvand, A., S. Hassanifard, S. Saadi, and A. Varvani-Farahani, Tensile properties and microstructural features of friction stir welded Al 6061 joints fabricated by various dual-pin tool shapes. Science and Technology of Welding and Joining, 2021. 26(6): p. 493502.

[6] Yang, J., D. Wang, B. Xiao, D. Ni, and Z. Ma, Effects of rotation rates on microstructure, mechanical properties, and fracture behavior of friction stir-welded (FSW) AZ31 magnesium alloy. Metallurgical and Materials Transactions A, 2013. 44(1): p. 517530.

[7] Devaiah, D., K. Kishore, and P. Laxminarayana, Optimal FSW process parameters for dissimilar aluminium alloys (AA5083 and AA6061) Using Taguchi Technique. Materials Today: Proceedings, 2018. 5(2): p. 46074614.

[8] Buffa, G., L. Fratini, F. Micari, and R. Shivpuri, Material flow in FSW of T-joints: experimental and numerical analysis. International Journal of Material Forming, 2008. 1(Suppl 1): p. 12831286.

[9] Sabet, H., M. Sadeghi, M. Sabet, H., M. Sadeghi, M. Mohammadikhah, N. Mirzamohammad, and M. Khalili, The Effect of Under Water Friction Stir Welding (UFSW) Variables on Microstructure and Mechanical Properties of 4343-Al Alloy Weld. 2011.

[10] Abbasi, M., A. Abdollahzadeh, B. Bagheri, A. Ostovari Moghaddam, F. Sharifi, and M. Dadaei, Study on the Effect of the Welding Environment

on the Dynamic Recrystallization Phenomenon and Residual Stresses During the Friction Stir Welding Process of Aluminum Alloy. Proceedings of the Institution of Mechanical Engineers, Part L: Journal of Materials: Design and Applications, 2021. 235(8): p. 18091826.

[11] Karimi Ivanaki, M., D. Afshari, E. Poursaeidi, and A. Bahrami, Experimental and numerical study of temperature and residual stress in two-pass friction stir welding of dissimilar alloys 6061-T6 to 5083. Proceedings of the Institution of Mechanical Engineers, Part B: Journal of Engineering Manufacture, 2025: p. 09544054251377157.

[12] Kim, C., D. Myung, D. Kim, and M.-G. Lee, Inhomogeneous flow stresses in FSW jointed aluminum alloy sheets inversely identified by FE-VFM. International Journal of Mechanical Sciences, 2023. 245: p. 108097.

[13] Zhang, H.-j. and Y. Lei, Thermal modeling of underwater friction stir welding of high strength aluminum alloy. Transactions of Nonferrous Metals Society of China, 2013. 23(4): p. 11141122.

[14] Chandran, R. and S.K.V. Santhanam, Submerged friction stir welding of 6061-T6 aluminium alloy under different water heads. Materials Research, 2018. 21: p. e20171070.

[15] Zhang, J., Y. Shen, X. Yao, H. Xu, and B. Li, Investigation on dissimilar underwater friction stir lap welding of 6061-T6 aluminum alloy to pure copper. Materials Design, 2014. 64: p. 7480.

[16] Sabari, S.S., S. Malarvizhi, V. Balasubramanian, and G.M. Reddy, Experimental and numerical investigation on under-water friction stir welding of armour grade AA2519-T87 aluminium alloy. Defence Technology, 2016. 12(4): p. 324333.

[17] Maharia, A.K., S. Sahu, and M. Zahid Ansari. Temperature and thermal stress distribution in underwater friction stir welding of aluminium plates. in IOP Conference Series: Materials Science and Engineering. 2018. IOP Publishing.

[18] Repplinger, C., S. Sellen, S. Kedziora, A. Zrbes, and S. Maas, Analysis of residual stress relaxation of aluminum alloys EN AW 6061/82 T6 under cyclic loading. Fatigue Fracture of Engineering Materials Structures, 2021. 44(11): p. 30233041.

[19] Salloomi, K.N. and S. Al-Sumaidae, Coupled EulerianLagrangian prediction of thermal and residual stress environments in dissimilar friction stir welding of aluminum alloys. Journal of Advanced Joining Processes, 2021. 3: p. 100052.

[20] Aval, H.J., S. Serajzadeh, and A. Kokabi, Evolution of microstructures and mechanical properties in similar and dissimilar friction stir welding of AA5086 and AA6061. Materials Science and Engineering: A, 2011. 528(28): p. 80718083.

[21] Schmidt, H., J. Hattel, and J. Wert, An analytical model for the heat generation in friction stir welding. Modelling and simulation in materials science and engineering, 2004. 12(1): p. 143157.